Materials Research. 2023; 26:e20220622
DOI: https://doi.org/10.1590/1980-5373-MR-2022-0622

Effect Synthesis Time of CeO_2 Nanoparticles by Microwave-Assisted Hydrothermal as a Sensing Device on CO Gas Sensitivity

Isabela Cristina Fernandes Vaz[a], *Ana Cristina Cabral*[a], *Alley Michael Silva Procópio*[a], *Hugo Marlon da Silva Nascimento*[a*], *Daniel Coelho do Amaral*[a], *Francisco Moura Filho*[a]

[a]*Universidade Federal de Itajubá, Laboratório de Materiais Avançados, Rua Irmã Ivone Drumond, 200, Distrito Industrial II, Itabira, MG, Brasil.*

Received: December 29, 2022; Revised: April 19, 2023; Accepted: May 11, 2023

The study presents CeO_2 particles synthesized by the microwave-assisted hydrothermal method using different synthesis times for the analysis of sensitivity to carbon monoxide gas, aiming at its application as a sensor material to prevent poisoning caused by this highly toxic gas. Structural, morphological and spectroscopic and electrical behaviors were analyzed by X-ray diffraction, Rietveld refinement, transmission electronic microscopy, Raman scattering spectroscopy, optoelectronic characterization chamber and FT-IR. The samples presented fluorite-type cubic structures, increase in crystallinity and particle size with the variation synthesis time from 5 to 8 minutes. From the micrographs it was observed that the nanoparticles initially were spherical with a surface domain (200), and the synthesis time made them cubic/polyhedral with a surface (111), showing differences in defects and influencing in its properties. The sample synthesized at 8 minutes showed the best result with response and recovery time of 16 and 2 seconds, respectively, at 390 °C, therefore promising for the fabrication of CO gas selective sensing device.

Keywords: *cerium dioxide, synthesis, microwave assisted hydrothermal method, carbon monoxide.*

1. Introduction

Cerium oxide (CeO_2) also called ceria is a promising compound for several technological applications mainly because its physical and chemical properties are easily modified through a control over the composition, type of structure, morphology, and size of the particles during its synthesis and process[1,2]. Some of the essential properties of this material are oxygen storage capacity, redox potential, thermal stability, chemical stability, low toxicity, electronic conductivity, and high oxygen mobility[3-5].

Studies report that the properties of CeO_2 nanocrystals are directly related to the morphological structure, particle size and the synthesis method[6,7]. Furthermore, CeO_2 has a fluorite-type cubic crystal structure, Fm3m space group, and a lattice parameter of 0.5411 nm at room temperature[8].

CeO_2 particles can be prepared by different routes, such as polymeric precursor method, sol-gel method, flow method, precipitation, organometallic decomposition, among others[9-14]. On the other hand, these chemical routes have some disadvantages, such as high temperatures, long processing times and the use of organic precursors/solvents[15]. Currently, two methods stand out in the preparation, growth and morphological control of different metallic oxides, conventional hydrothermal (HT) and microwave-assisted hydrothermal (MAH) methods[15,16]. Studies report that MAH has great advantages, below 200 ºC it is possible to obtain pure oxides, high crystallinity, various morphologies, low processing/synthesis time and energy[8,17].

Therefore, the combination of CeO_2 physicochemical properties makes it a versatile material with a range of applications, such as optical devices, catalysts, solid oxide fuel cells, hydrogen storage materials, gas sensor, among others[18-28]. Oliveira et al.[7] studied morphological, optical and electronic properties of cerium oxide varying the synthesis time by the microwave-assisted hydrothermal method. It was observed that CeO_2 nanoparticles when exposed to a dry air atmosphere increases the electrical resistance of the material, and when exposed to a vacuum atmosphere the electrical resistance decreases as a temperature function and morphologies found in the samples. These researchers concluded that vacuum promotes oxygen desorption on the CeO_2 nanoparticles surface, and that the electrons loss in the 4f state of cerium causes a reduction in electrical resistance. López-Mena et al.[3] synthesized nanostructured CeO_2 microspheres by co-precipitation, testing their application in carbon monoxide detection. They obtained a response time of 9 s at 275 °C, for the 200 ppm CO detection at a 100 kHz frequency. The result revealed that the CeO_2 material showed a reproducible and stable detection response.

In this work, we discuss the obtainment and characterization of CeO_2 powders synthesized by the MAH method and the thick films preparation of these powders to evaluate their response as a possible sensor material in CO detection; and also, to link these responses to material-induced changes in synthesis time.

*e-mail: hugomarlondasilva@gmail.com

2. Materials and Methods

2.1. Synthesis and characterization of the CeO_2

CeO_2 powders were prepared by microwave assisted hydrothermal method. $Ce(NO_3)_3.6H_2O$ (99.9% purity, Sigma-Aldrich) was dissolved in deionized water under constant stirring. To this solution, we slowly add, until pH 10, a few **1 M** KOH solution milliliters. The system obtained was heat treated with the aid of a domestic microwave (2.45 GHz, maximum power of 800 W) adapted with a Teflon autoclave. For the process, a temperature of 100 °C was used, with a heating rate of 10 °C min^{-1} in 5 and 8 min times. Subsequently, the autoclave was cooled to room temperature and then the CeO_2 powders were collected and washed with deionized water several times, and dried at 100 °C in an oven.

For the characterization of the crystalline structure of the powders, a diffractometer was used, with a copper tube (λ = 1.5406 Å) in a range from 20° to 110° with 1° min^{-1}. Rietveld refinement was made with the software GSAS (General Structure Analysis System)[29] and the graphical user interface EXPGUI developed by B. H. Toby[30]. Morphological structure analysis of the films was performed by transmission electron microscopy (TEM) on a FEI instrument. For this, the samples were previously dispersed in ethanol, sprayed on Cu grids (300 mesh) and finally dried.

To identify the functional groups, present in the samples which would indicate the presence of possible second phases which in turn could degrade the electrical property. In this work, Fourier transform infrared absorption spectroscopy (FT-IR) was performed using a Perkin Elmer Frontier model spectrometer in transmittance mode. The spectra were measured with 64 scans in the region between 4000 cm^{-1} and 400 cm^{-1} using a resolution of 1 cm^{-1}. All these measurements were made at room temperature.

2.2. Preparation and characterization of the sensor device

Initially, a paste containing cerium oxide powders and binder (glycerol) was prepared. Powder/binder ratio was 1.6 g mL^{-1}. Then, this paste was deposited on an alumina substrate with interdigitated platinum electrodes. After deposition, the films were dried at 100 °C for 24 h in a dry air atmosphere to evaporate the binder. Subsequently, the heat was treated in a dry air atmosphere with steps of 1 °C min^{-1} to 380 °C and maintained at this temperature for 2 h to evaporate the residual binder or any impurities presented.

Raman scattering spectroscopy was performed in a Synapse spectrometer (HORIBA Jobin Yvon, France), 32 scans in the region from 200 to 800 cm^{-1} and 4 cm^{-1} spectral resolution, coupled with an optical microscope model BX41 (Olympus, Japan) and equipped with an Nd-YAG laser (λ = 514.5 nm), operated at 100 mW.

To perform the electrical measurements, an optoelectronic characterization chamber formed in a closed chamber was used[31,32]. In it, three measurements of electrical response of heating and cooling as a function of temperature were performed, in which vacuum, air and CO environments were chosen under 50 mmHg constant pressure.

3. Results and Discussion

XRD patterns and structural refinement for CeO_2 nanoparticles obtained at 100 °C for 5 to 8 **min** are shown in Figure 1. Figure 1a indicates samples monophasic with a fluorite-type cubic structure and Fm3m space group[33]. All diffraction peaks conform to the Inorganic Crystal Structure Database (ICSD) card nº 72155[34]. The sample obtained in 5 **min** has sharp but broad diffraction peaks indicating to be composed of small poor crystallinity primary particles. Meanwhile, the sample obtained in 8 **min** presents narrow peaks characteristic with the presence of larger particles and good crystallinity. Table 1 reports the experimental data of Rietveld refinement. Data show that the lattice parameters and unit cell volumes are close to the values published in the literature[35-37] and a Joint Committee on Powder Diffraction Standards (JCPDS) card nº 34-0394 for CeO_2 powder where the theoretical lattice parameter was 5.411 Å [38]. An increase in the lattice parameter and unit cell volume is observed, which is normally associated with the synthesis time that influences the particle growth mechanism and, consequently, changes in morphology, crystallinity and deformation of the compound[7]. There is an association between the observed experimental XRD patterns and the theoretical, which can be observed by the same parameter GoF. **To explain the growth of CeO_2 particles for hydrothermal conditions two mechanisms are proposed by the literature: Ostwald ripening (OR) and oriented fixation (OA).** The OA mechanism took place through the effective collision of cores, using the same crystallographic orientation responsible for obtaining the primary particles of low crystallinity. The OR process required more time to dissolve and recrystallize the material into a larger crystal, increasing crystallinity and reducing defects and surface energy. OA mechanism was the dominant process in this synthesis method, because of the microwave radiation, leading to anisotropic growth of nanoparticles, for the electrostatic interactions in the colloidal system. More time used, there was clearer concision to control the recrystallization process, having the OR mechanism[7,39]. Therefore, the increase in synthesis time increases the crystallinity of the nanoparticles (Figure 1b, c), and this caused a variation in the structural defects, that is, in the oxygen vacancies, distortion in the bonds, tensions and deformations in the crystal lattice, in addition, it affected the surface defects that influence the material's sensing properties.

Morphology and particle size of the samples were examined by TEM. Figure 2a, c shows CeO_2 nanoparticles

Table 1. Lattice parameters and quality indices of the Rietveld refinement of CeO_2 nanoparticles.

Refined formula (CeO_2)	Lattice parameters		Unit cell volume (Å^3)	R_B (%)	GoF(%)	R_{wp} (%)	R_{exp} (%)
	a = b = c (Å)	$\alpha = \beta = \gamma$					
5 min.	5.4134 (6)	90	158.64 (6)	3.06	1.05	12.18	9.04
8 min.	5.4175 (6)	90	159.00 (5)	4.70	1.49	5.29	4.23

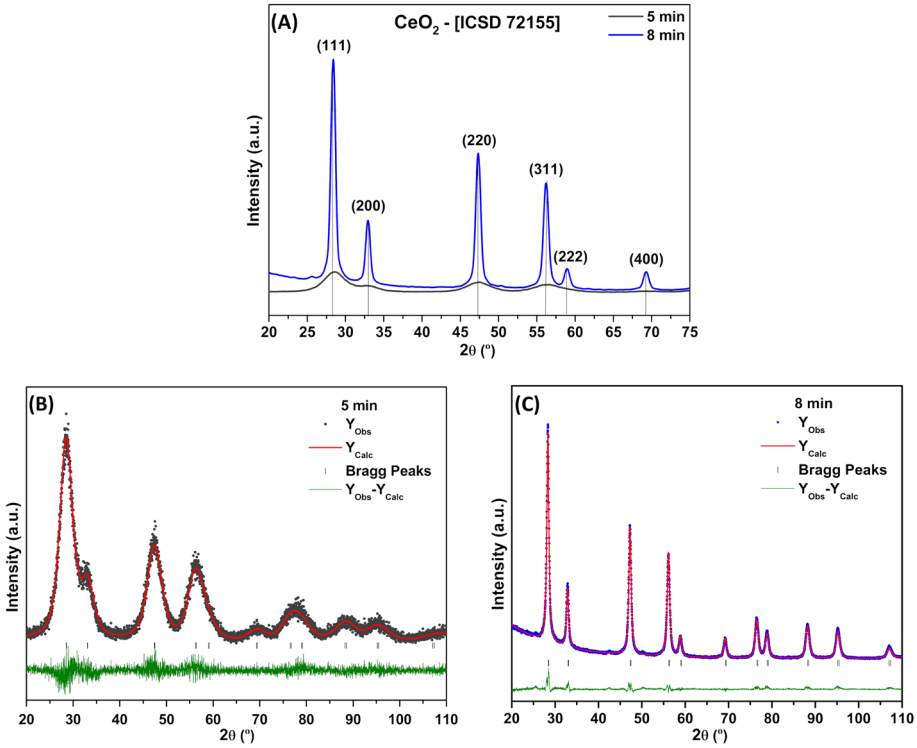

Figure 1. a) XRD patterns of the CeO_2 nanoparticles synthesized at 100 °C for 5 and 8 minutes by MAH method; Rietveld refinement; b) synthesis for 5 minutes; c) synthesis for 8 minutes.

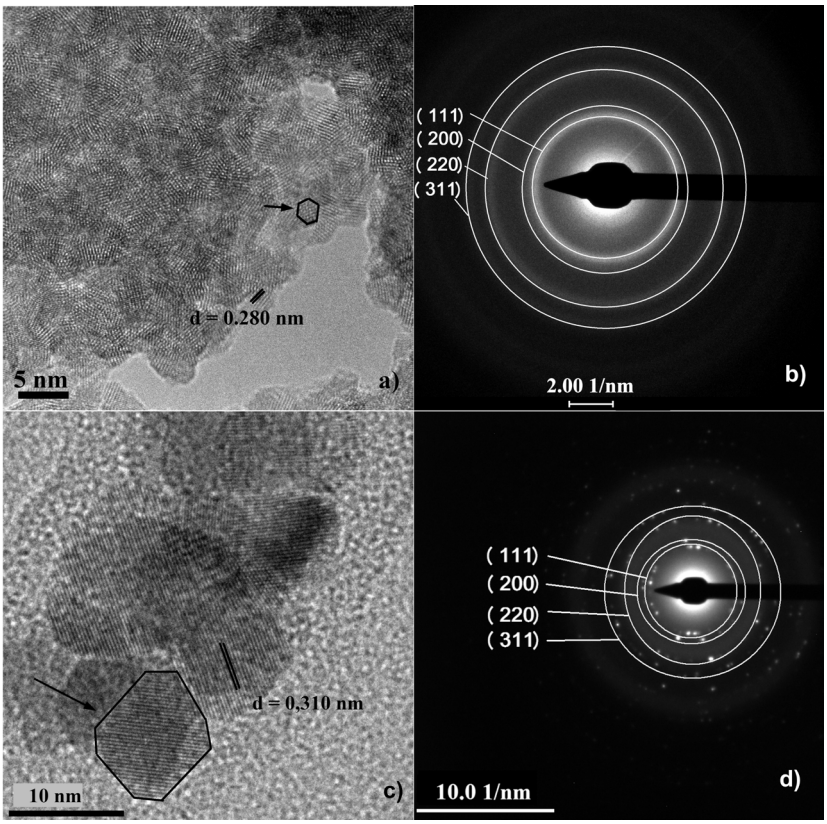

Figure 2. TEM micrographs of the CeO_2 nanoparticles synthesized at 100 °C f by MAH method; a) 5 min; (c) 8 min; SAED micrographs; b) 5 min; (d) 8 min.

using 5 and 8 min with average particle size of 5 and 10 nm, respectively. In addition, agglomerated particles were observed using water as a solvent[36]. These agglomerates were formed by the small size of the particles, and high-density defects and energy. As time was added, particle size enlarged, and reduced surface free energy[7]. Figure 2a shows typical characteristics of the OA process. In this figure, we can observe a mesocrystal-like structure with clear boundaries compared to the oriented primary particles. Using more time (Figure 2c), the presence of the grain boundary became less evident, presenting a more regular surface, indicating the occurrence of self-recrystallization[39].

The recorded SAEDs patterns (Figure 2b, d) corroborate the XRD result, that the samples are crystalline belonging to the fluorite-type cubic structure. The spaces of the lattice fringes were 0.280 and 0.310 nm (Figure 2b, d) for the CeO_2 synthesized in 5 and 8 min, respectively, calculated from the TEM images correspond to the (200) and (111) lattice planes of a fluorite-type cubic structure[35]. Adding time to the synthesis, nanoparticles agglomerate **tends** to organize themselves to form polyhedral/cube. Considering that, crystal morphologies grow from the ideal crystal (111), we can conclude that the facets (111) of the samples were exposed to minimize the particles surface energy. So, a polyhedron morphology was obtained by adding time, and the particles form ideal cubes or crystals[7,39]. Defects of different types can be found on each exposed surface, for example, surface (111) needs more energy to form facets (100). Therefore, we can observe that the synthesis time changes the concentration of surface defects, one of which is the oxygen vacancies, contributing to the detection properties, as reported by Maekawa et al.[40].

Figure 3 shows the FT-Raman spectrum of the CeO_2 film. Active Raman vibrational modes are observed in the range between 200-1000 cm^{-1}**.** Main Raman (F_{2g}) mode referred to an intense peak located at approximately 449 and 462 cm^{-1}, for 5 min and 8 min, respectively, and was attributed to the symmetrical vibration mode of elongation of the oxygen atoms around each cerium atom[41]. According to the literature[42], the fluorite-like cubic structure of cerium oxide presents a triply degenerate F_{2g} mode at ~465 cm^{-1} displacements, being shifted to smaller particles. Ceria nanoparticles prepared by the microwave-assisted solvothermal method[43] showed bands shifted to a lower frequency, this effect being explained by the expansion of the lattice with the decrease in its size. The lower intensity bands around 250 cm^{-1} and 600 cm^{-1} were more pronounced in the sample 5 min and were attributed in the literature to short-range structural defects, the most common being oxygen vacancies. As the synthesis time was added, the modes got thin and the additional peaks practically disappeared, indicating more short-range structural ordering[7,44,45].

Vibration mode at 830 cm^{-1} indicates that there is a reduction from Ce^{4+} to Ce^{3+} in the samples, as this band is related to the change in short-range symmetry. As this oxide reduction reaction is associated with the defect's generation such as oxygen vacancies, it can be said that this defect type is present in the material structure[28]. Therefore, a higher rate of oxygen diffusion rate in the network is favored by the presence of oxygen vacancies, to assist in the process reduction from Ce^{4+} to Ce^{3+}, and occurs for the shortest synthesis time[7]. However, the presence of these defects influences the electrical properties of the material, as can be seen in Figure 4 regarding the electrical resistance analyses.

Figure 4 presents the electrical transport of CeO_2 nanoparticles in relation to the n-type semiconductor behavior. Ionized and adsorbed O_2^-, O^- and O^{2-} species formation occurs due to the great availability of unpaired electrons from the oxygen vacancies existing on the sensor device surface[46,47]. According to Equations 1-3, oxygen species adsorbed on the material surface react with CO molecules, oxidizing them to CO_2, releasing electrons in the conduction band, which reduces the electrical resistance of the sensor device[48,49].

$$2CO + O_2^- \rightarrow 2CO_2 + e^- \qquad (T < 100\,°C) \qquad (1)$$

$$CO + O^- \rightarrow CO_2 + e^- \qquad (100\,°C < T < 300\,°C) \qquad (2)$$

$$CO + O^{2-} \rightarrow CO_2 + 2e^- \qquad (T > 300\,°C) \qquad (3)$$

Figure 4a illustrates the relative resistance evaluated from the expression R_{VAC}/R_{CO} in temperature function for thick films, where R_{VAC} is resistance in the vacuum atmosphere and R_{CO} is resistance in the CO atmosphere[50]. Sample synthesized in 8 min showed exponentially higher relative resistance

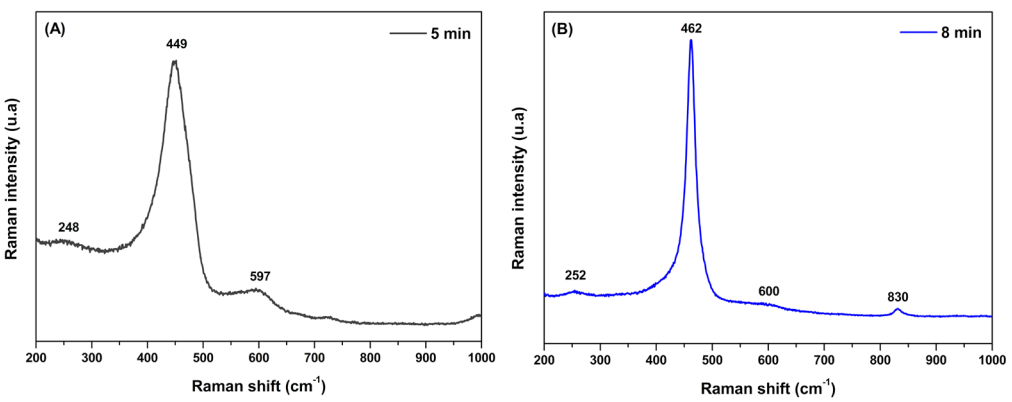

Figure 3. Raman spectra of CeO_2 nanoparticles synthesized at 100 °C for (a) 5 min and (b) 8 min in the MAH method.

for temperatures >320 °C, having a greater response when compared to sample synthesized in 5 min, with lower R_{CO} values. Relative resistance was obtained at a maximum value at 390 °C for a relative resistance of ~25, this sensor device working temperature value is close to those reported in the literature[28]. Therefore, CO gas causes oxygen desorption on the sample surface, as well as the vacuum atmosphere pointed out by Oliveira et al.[7], generating less electrons in the 4f state of Ce as well as electrical resistance of the sample. The authors emphasized that this effect depends on the different surfaces, such as the exposed faces, obtained in the nanoparticles according to the synthesis time used. They observed a reduction in the samples obtained with times longer than 8 min of synthesis using a temperature of 180 °C in the MAH method. In addition, López-Mena et al.[3] concluded that less agglomerated particles presented better electrical response. That´s may be the reason why the sample obtained in shorter synthesis time did not show a good result.

Arrhenius Law associated with linear regression (Figure 4b) was used to define the activation energy (Ea) using a vacuum atmosphere to ensure that gas adsorption/desorption and oxygen diffusion do not occur during heating and cooling processes[51]. Ea values for the samples synthesized for 5 and 8 min were 0.39 eV and 0.30 eV, respectively. Results that corroborate with Figure 4a, where the sample synthesized in 8 min showed better electrical response to gas. Electrical response is due to the contribution of different levels of intermediate energy within the band gap, related to the electron in the 4f orbital of cerium, being the probable cause of the formation of surface defects, such as oxygen vacancies, resulting from changes in morphology of the film nanoparticles. For the sample synthesized in 8 min, surface dominance (111) was observed with the presence of only one oxygen vacancy, which forms more stable holes that reduce the electrical resistance in the CO atmosphere. Whereas the 5 min sample had a surface domain (200) with two oxygen vacancies stabilizing the electron/hole pair[7].

Once the working temperature (Figure 4c) was determined, we studied the resistance behavior as a time function at 390 °C, for the thick film of the sample synthesized at 8 min. This analysis was performed by alternating the atmosphere from synthetic air (~20% oxygen) to vacuum and 50 mmHg of CO (99.99%). The response/recovery time was investigated when exposed to CO gas, and the values were 16 s and 2 s, respectively, lower than that reported by Ortega **et** al.[49], using a different CeO_2 precursor because of the presence of more oxygen vacancies[52]. Response time is defined as the period of time the material takes to use its resistance by 90% of the initial value when exposed to the target gas. Recovery time, on the other hand, is the time required to recover 90% of initial strength after exposure to the gas. For this material, the electrical conduction mechanism is dominated by the tunneling current, in which defects are created with the presence of oxygen vacancies, which allows, in the 4f states of Ce, an increase in the number of electrons. When an electron goes to the $4f^0$ state of Ce due to the process of vacancy formation, we observe a reduction in electrical resistance[7,53]. Therefore, the effect attributed to the morphology of this sample, which formed polyhedral/cubes with exposed faces that had more stable defects, improved the material sensitivity.

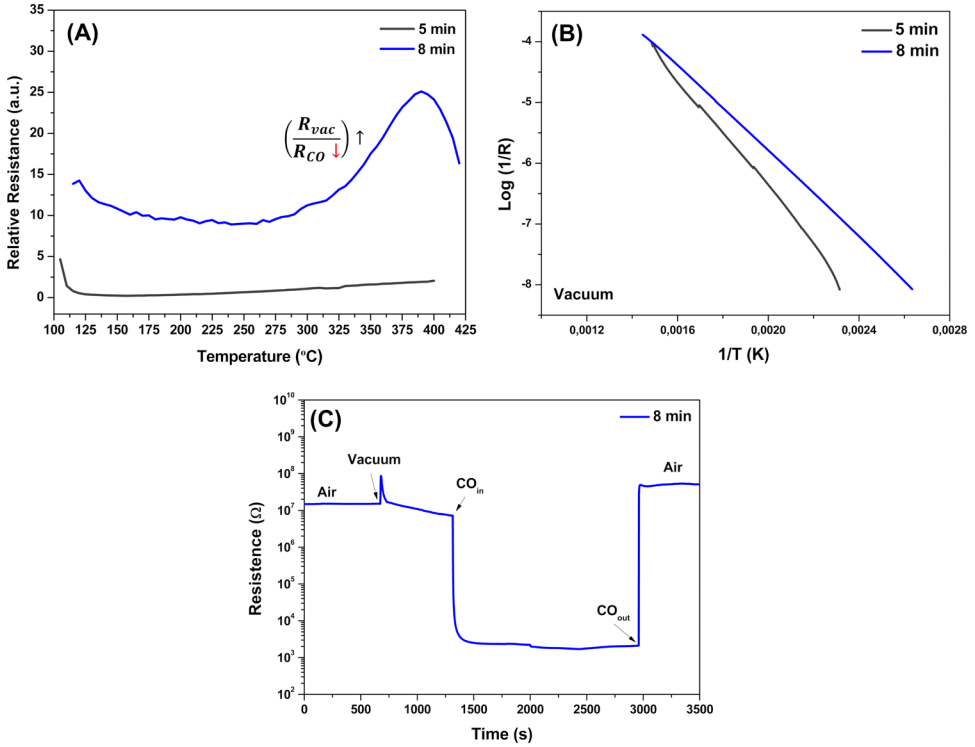

Figure 4. Electrical measurements; a) relative resistance vs temperature; b) conductance during cooling (vacuum atmosphere); c) electrical resistance as a function of time in different atmospheres for the CeO_2 sensor films synthesized at 100 °C by the MAH method.

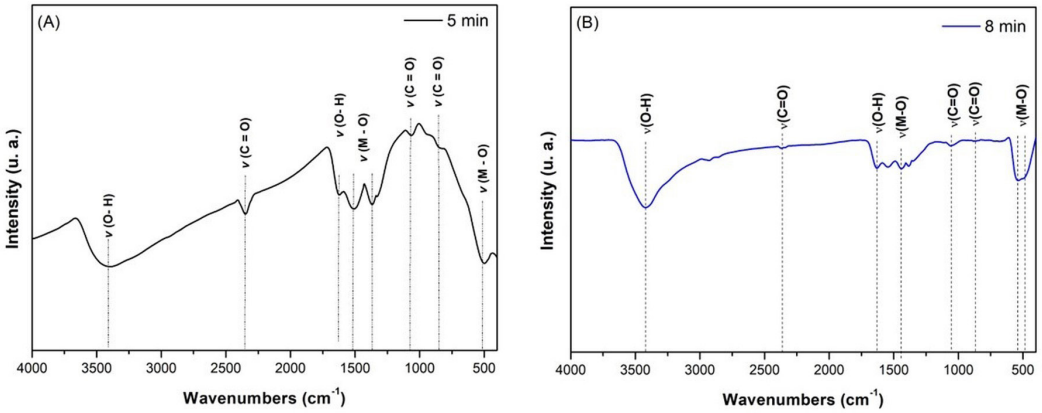

Figure 5. FT-IR spectra of CeO_2 nanoparticles synthesized at 100 °C for (a) 5 min and (b) 8 min in the MAH method.

Figure 5 illustrates the vibrational spectra in the infrared region of CeO_2 powders, in the region from 400 cm^{-1} to 4000 cm^{-1}, both samples show bands at the same wavelengths, the differences in spectral configuration can be attributed to higher crystallinity of the sample formed after 8 min. According to group theory, CeO_2 has 2 active modes in the infrared region that are triply degenerate with two cluster-related absorption bands [CeO_8]. The two bands located at 1500 cm^{-1} and 1300 cm^{-1} are asymmetric stretching vibrations of Metal – O bonds [54,55]. On the other hand, the symmetric bending modes corresponding to these connections were verified around 500 cm^{-1} [54,56,57]. The other bands attributed to the metal-oxygen bond were not detected due to the spectral limit of the equipment, since they are located in wavenumbers lower than 400 cm^{-1} [56]. Other absorption bands were found in the spectra of these powders. The bands around 3400 cm^{-1} are attributed to the stretching vibration of the O – H bonds due to moisture adsorbed on the surface of the sample wafer in KBr and are accompanied by a band at and 1600 cm^{-1} due to angular deformation of H – O – H [55-58]. The band around 2300 cm^{-1} comes from carbon dioxide (CO_2) adsorbed on metallic cations, due to the C = O stretching vibration of CO_2 present in the air, as well as those observed in the region at about 1000 cm^{-1} [54,58-60]. The weak bands around 1600, 1500 and 1000 cm^{-1} are similar to the FT-IR spectra of commercial powders of CeO_2 nanoparticles[54,55]. Thus, it is confirmed that cerium oxide nanocrystals were indeed formed during MAH synthesis.

4. Conclusions

Crystalline and monophasic CeO_2 nanoparticles with a fluorite-type cubic structure were synthesized by MAH method according to the results of XRD, Rietveld refinement, Raman and TEM analysis. Increasing the synthesis time, particles with greater crystallinity were less agglomerated, and the transformation from a polyhedral morphology in an exposed (110) surface to a cubic morphology in an exposed surface (100) surface was observed. The response time of 16 s at 390 °C, indicated that the defective structure of CeO_2-based materials provided mechanisms for its application, based on the transient $4f^1$ electrons of Ce that can migrate through tunneling/jumping mechanisms because of the redox processes that may occur.

5. Acknowledgments

We thank LIMAv/Unifei and LIEC/UFSCar for the necessary infrastructure to carry out this research and to CNPq, FAPEMIG and CAPES for the financial support.

6. References

1. Wang G, Um Q, Chen T, Wang Y. Synthesis, characterization and photoluminescence of CeO_2 nanoparticles by a facile method at room temperature. J Alloys Compd. 2010;493:202-7. http://dx.doi.org/10.1016/j.jallcom.2009.12.053.
2. Liu B, Liu B, Li Q, Li Z, Yao M, Liu R, et al. High-pressure Raman study on CeO_2 nanospheres self-assembled by 5 nm CeO_2 nanoparticles. Phys Status Solidi, B Basic Res. 2011;248:1154-7. http://dx.doi.org/10.1002/pssb.201000807.
3. López-Mena ER, Michel CR, Martínez-Preciado AH, Elías-Zuñiga A. Simple route to obtain nanostructured CeO_2 microspheres and CO gas sensing performance. Nanoscale Res Lett. 2017;12:169-78. http://dx.doi.org/10.1186/s11671-017-1951-x.
4. Procópio AMS, Carvalho JDL, Silveira THR, Valério AL, Vaz ICF, Cabral ACT, et al. CeO_2 thin film supported on TiO_2 porous ceramics. Mater Lett. 2020;276:128224. http://dx.doi.org/ 10.1016/j.matlet.2020.128224.
5. Carvalho JCL, Rocha LSR, Renzetti RA, Procopio AMS, Mastelaro VR, Simoes AZ, et al. High-performance CeO_2:Co nanostructures for the elimination of accidental poisoning caused by CO intoxication. Open Ceramics. 2022;12:100298. http://dx.doi.org/10.1016/j.oceram.2022.100298.
6. Arasu MV, Thirumamagal R, Srinivasan MP, Al-Dhabia NA, Ayeshamariam A, Kumar DS, et al. Green chemical approach towards the synthesis of CeO_2 doped with seashell and its bacterial applications intermediated with fruit extracts. J Photochem Photobiol B. 2017;173:50-60. http://dx.doi.org/10.1016/j.jphotobiol.2017.05.032.
7. Oliveira RC, Amoresi RAC, Marana NL, Zaghete MA, Ponce M, Chiquito AJ, et al. Influence of synthesis time on the morphology and properties of CeO_2 nanoparticles: an experimental–theoretical study. Cryst Growth Des. 2020;20:5031-42. http://dx.doi.org/10.1021/acs.cgd.0c00165.
8. Shannon RD. Revised effective ionic radii and systematic studies of interatomic distances in halides and chalcogenides. Acta Crystallogr A. 1976;32:751-67. http://dx.doi.org/ 10.1107/S0567739476001551.
9. Meng F, Wang L, Cui J. Controllable synthesis and optical properties of nano-CeO_2 via a facile hydrothermal route. J Alloys Compd. 2013;556:102-8. http://dx.doi.org/10.1016/j.jallcom.2012.12.096.

10. Meng T, Ara M, Wang L, Naik R, Simon KY. Enhanced capacity for lithium-air batteries using $LaFe_{0,5}Mn_{0,5}O_3$-CeO_2 composite catalyst. J Mater Sci. 2014;49:4058-66. http://dx.doi.org/10.1007/s10853-014-8070-1.
11. Rocha RA, Muccillo ENS. Preparation and characterization of $Ce_{0,8}Gd_{0,2}O_{1,9}$ solid electrolyte by polimeric precursor techniques. Mater Sci Forum. 2003;416-418:711-9. http://dx.doi.org/10.4028/www.scientific.net/MSF.416-418.711.
12. Bondioli F, Corradi AB, Manfredini T, Leonelli G, Bertoncello R. Nonconventional synthesis of praseodymium-doped ceria by flux method. Chem Mater. 2000;12:324-30. http://dx.doi.org/10.1021/cm990128j.
13. Song HZ, Wang HB, Zha SW, Peng DK, Meng GY. Aerosol-assisted MOCVD growth of Gd_2O_3-doped CeO_2 thin SOFC electrolyte film on anode substrate. Solid State Ion. 2003;156:249-54. http://dx.doi.org/10.1016/S0167-2738(02)00688-4.
14. Thangadurai V, Kopp P. Chemical synthesis of Ca-doped CeO_2-intermediate temperature oxide ion electrolytes. J Power Sources. 2007;168:178-83. http://dx.doi.org/ 10.1016/j.jpowsour.2007.03.030.
15. Cavalcante LS, Sczancoski JC, Siu Li M, Longo E, Varela JA. β-$ZnMoO_4$ microcrystals synthesized by the surfactant-assisted hydrothermal method: growth process and photoluminescence properties. Colloids Surf A Physicochem Eng Asp. 2012;396:346-51. http://dx.doi.org/10.1016/j.colsurfa.2011.12.021.
16. Oliveira LL, Cortés JA, Caldeira BS, Strusch T, Wiedwald U, Simões AZ. Structural, electronic paramagnetic resonance and magnetic properties of praseodymium-doped rare earth CeO_2 semiconductors. Ceram Int. 2021;47:20768-80. http://dx.doi.org/10.1016/j.ceramint.2021.04.133.
17. Deus RC, Foschini CR, Spitova B, Moura F, Longo E, Simões AZ. Effect of soaking time on the photoluminescence properties of cerium oxide nanoparticles. Ceram Int. 2014;40:1-9. http://dx.doi.org/10.1016/j.ceramint.2013.06.043.
18. Reddy BM, Khan A, Yamada Y, Kobayashi T, Loridant S, Volta JC. Raman and X-ray photoelectron spectroscopy study of CeO_2-ZrO_2 and V_2O_5/CeO_2-ZrO_2 catalysts. Langmuir. 2003;19:3025-30. http://dx.doi.org/10.1021/la0208528.
19. Bera P, Gayen A, Hegde MS, Lalla NP, Spadaro L, Frusteri F, et al. Promoting effect of CeO_2 in combustion synthesized Pt/CeO_2 catalyst for CO oxidation. J Phys Chem B. 2003;107:6122-30. http://dx.doi.org/10.1021/jp022132f.
20. Jacobs G, Willians L, Graham U, Sparks D, Davis BH. Low-temperature water-gas shift: in-situ DRIFTS – reaction study of a Pt/CeO_2 catalyst for fuel cell reformer applications. J Phys Chem B. 2003;107:10398-404. http://dx.doi.org/10.1021/jp0302055.
21. Li RX, Yabe S, Yamashida M, Momose S, Yoshida S, Yin S, et al. Synthesis and UV-shielding properties of ZnO- and CaO-doped CeO_2 via soft solution chemical process. Solid State Ion. 2002;151:235-41. http://dx.doi.org/10.1016/S0167-2738(02)00715-4.
22. Sohlberg K, Pantelides ST, Pennycook SJ. Interactions of hydrogen with CeO_2. J Am Chem Soc. 2001;123:6609-11. http://dx.doi.org/10.1021/ja004008k.
23. Jasinki P, Suzuki T, Anderson HU. Nanocrystalline undoped ceria oxygen sensor. Sens Actuators B Chem. 2003;95:73-7. http://dx.doi.org/10.1016/S0925-4005(03)00407-6.
24. Goubin F, Rocquefelt X, Whangbo MH, Montardi Y, Brec R, Jobic S. Experimental and theorical characterization of the optical properties of CeO_2, $SrCeO_3$, and Sr_2CeO_4 containing Ce^{4+} (f^0) ions. Chem Mater. 2004;16:662-9. http://dx.doi.org/10.1021/cm034618u.
25. Shchukin DG, Caruso RA. Template synthesis and photocatalytic properties of porous metal oxide spheres formed by nanoparticle infiltration. Chem Mater. 2004;16:2287-92. http://dx.doi.org/10.1021/cm0497780.
26. Arul NS, Mangalaraj D, Ramachandran R, Grace AN, Han JI. Fabriccation of CeO_2/Fe_2O_3 composite nanospindles for enhanced visible light driven photocatalysts and supercapacitor electrodes. J Mater Chem A Mater Energy Sustain. 2015;29:15248-58. http://dx.doi.org/10.1039/C5TA02630J.
27. Sun C, Li H, Chen L. Nanostructured ceria-based materials: synthesis, properties, and applications. Energy Environ Sci. 2012;5:8475-505. http://dx.doi.org/10.1039/C2EE22310D.
28. Rocha LSR, Amoresi RAC, Moreno H, Ramirez MA, Ponce MA, Foschini CR, et al. Novel approaches of nanoceria with magnetic, photoluminescent, and gas-sensing properties. ACS Omega. 2020;5:14879-89. http://dx.doi.org/10.1021/acsomega.9b04250.
29. Larson AC, Von Dreele RB. General structure analysis system (GSAS). Los Alamos: Los Alamos National Laboratory; 2004. Report No. LAUR 86-748.
30. Toby BH. EXPGUI, a graphical user interface for GSAS. J Appl Cryst. 2001;34:210-3. http://dx.doi.org/10.1107/S0021889801002242.
31. Tibaldi N, Ponce MA, Kalafatovich P, Asencio H, Desimone MP, Simões AZ, et al. Dispositivo para caracterización optoelectrónica de materiales. Argentina Patent n°. 20150103953, 2015.
32. Tibaldi N, Ponce MA, Kalafatovich P, Asencio H, Desimone MP, Simões AZ, et al. Dispositivo de caracterização optoeletrônica de materiais. Brazil Patent n°. BR 10 2016 028383 3, 2016.
33. Wolcyrz M, Kepinski L. Rietveld refinement of the structure of CeOCI formed in Pd/CeO_2 catalyst: notes on the existence of a stabilized tetragonal phase of La_2O_3 in La-Pd-O system. J Solid State Chem. 1992;99:409-13. http://dx.doi.org/10.1016/0022-4596(92)90330-X.
34. Hwang G, Choi J. Determination of crystal size and microstrain of CeO_2 by Rietveld structure refinement. J Mineralogical Soc Korea. 2008;21:201-8.
35. Wang G, Mu Q, Chen T, Wang Y. Synthesis, characterization and photoluminescence of CeO_2 nanoparticles by a facile method at room temperature. J Alloys Compd. 2010;493:202-7. http://dx.doi.org/10.1016/j.jallcom.2009.12.053.
36. Deus RC, Cilense M, Foschini CR, Ramirez MA, Longo E, Simões AZ. Influence of mineralizer agents on the growth of crystalline CeO_2 nanospheres by the microwave-hydrothermal method. J Alloys Compd. 2013;550:245-51. http://dx.doi.org/10.1016/j.jallcom.2012.10.001.
37. Jayababu N, Poloju M, Shruthi J, Reddy MR. NiO decorated CeO2 nanostructures as room temperature isopropanol gas sensors. RSC Adv. 2019;24:13765-775. http://dx.doi.org/10.1039/C9RA00441F.
38. Ikuma Y, Anandan S, Niwa K. Lattice parameter, defect concentration and oxygen diffusion in ceria solid solutions. Trans Mater Res Soc Jpn. 2010;35:485-9. http://dx.doi.org/10.14723/tmrsj.35.485.
39. Dalmaschio CJ, Ribeiro C, Leite ER. Impact of the colloidal state on the oriented attachment growth mechanism. Nanoscale. 2010;2:2336-45. http://dx.doi.org/10.1039/C0NR00338G.
40. Maekawa T, Suzuki K, Takada T, Kobayashi T, Egashira M. Odor identification using a SnO_2-based sensor array. Sens Actuators B Chem. 2001;80:51-8. http://dx.doi.org/10.1016/S0925-4005(01)00885-1.
41. Lu F, Meng F, Wang L, Sang Y, Luo J. Controlled synthesis and optical properties of CeO_2 nanoparticles by a $N_2H_4.H_2O$-assisted hydrothermal method. Micro & Nano Lett. 2012;7:624-7. http://dx.doi.org/10.1049/mnl.2012.0279.
42. Zhang YW, Rui S, Liao CS, Yan CH. Facile alcohothermal synthesis, size-dependent ultraviolet absorption, and enhanced CO conversion activity of ceria nanocrystals. J Phys Chem B. 2003;107:10159-67. http://dx.doi.org/10.1021/jp034981o.
43. Martins TS, Isolani PC. Terras raras: aplicações industriais e biológicas. Quim Nova. 2005;28:111-7. http://dx.doi.org/10.1590/S0100-40422005000100020.

44. Nottbohm CT, Hess C. Investigation of ceria by combined Raman, UV–vis and X-ray photoelectron spectroscopy. Catal Commun. 2012;22:39-42. http://dx.doi.org/10.1016/j.catcom.2012.02.009.
45. Pushkarev VV, Kovalchuk VI, D'Itri JL. Probing defect sites on the CeO_2 surface with dioxygen. J Phys Chem B. 2004;108:5341-8. http://dx.doi.org/10.1021/jp0311254.
46. Liu F, Wang X, Chen X, Song X, Tian J, Cui H. Porous ZnO ultrathin nanosheets with high specific surface areas and abundant oxygen vacancies for acetylacetone gas sensing. ACS Appl Mater Interfaces. 2019;11:24757-63. http://dx.doi.org/10.1021/acsami.9b06701.
47. Li P, Wang B, Li W, Qin C, Sun L, Wu N, et al. Effect of annealing atmosphere with different oxygen concentration on CO gas sensing performances for CeO_2 nanoparticles. Mater Lett. 2021;284:129000. http://dx.doi.org/10.1016/j.matlet.2020.129000.
48. Durrani SMA, Al-Huhaili MF, Bakhtiari IA. Carbon monoxide gas-sensing properties of electron-beam deposited cerium oxide thin films. Sens Actuators B Chem. 2008;134:934-9. http://dx.doi.org/10.1016/j.snb.2008.06.049.
49. Ortega PP, Rocha LSR, Cortés JA, Ramirez MA, Buono C, Ponce MA, et al. Towards carbon monoxide sensors based on europium doped cerium dioxide. Appl Surf Sci. 2019;464:692-9. http://dx.doi.org/10.1016/j.apsusc.2018.09.142.
50. Nandy T, Coutu RA Jr, Ababei C. Carbon monoxide sensing technologies for next-generation cyber-physical systems. Sensors (Basel). 2018;18:3443. http://dx.doi.org/10.3390/s18103443.
51. Deus RC, Amoresi RAC, Desimone PM, Schipani F, Rocha LSR, Ponce MA, et al. Electrical behavior of cerium dioxide films exposed to different gases atmospheres. Ceram Int. 2016;42:15023-9. http://dx.doi.org/10.1016/j.ceramint.2016.06.151.
52. Oliveira RC, Cabral L, Cabral AC, Almeida PB, Tibaldi N, Sambrano JR, et al. Charge transfer in Pr-Doped cerium oxide: experimental and theoretical investigations. Mater Chem Phys. 2020;249:122967. http://dx.doi.org/10.1016/j.matchemphys.2020.122967.
53. Nolan M, Grigoleit S, Sayle DC, Parker SC, Watson GW. Density functional theory studies of the structure and electronic structure of pure and defective low index surfaces of ceria. Surf Sci. 2005;576(1-3):217-29. http://dx.doi.org/10.1016/j.susc.2004.12.016.
54. Palard M, Balencie J, Maguer A, Hochepied J-F. Effect of hydrothermal ripening on the photoluminescence properties of pure and doped cerium oxide nanoparticles. Mater Chem Phys. 2010;120:79-88. http://dx.doi.org/10.1016/j.matchemphys.2009.10.025.
55. Wang G, Mu Q, Chen T, Wang Y. Synthesis, characterization and photoluminescence of CeO_2 nanoparticles by a facile method at room temperature. J Alloys Compd. 2010;493:202-7. http://dx.doi.org/10.1016/j.jallcom.2009.12.053.
56. Farahmandjou ME, Zarinkamar M. Synthesis of nano-sized ceria (CeO_2) particles via a cerium hydroxy carbonate precursor and the effect of reaction temperature on particle morphology. J Ultrafine Grained Nanostruct Mater. 2015;48:5-10. http://dx.doi.org/10.7508/JUFGNSM.2015.01.002.
57. Ponnaiah SK, Periakaruppan P, Vellaichamy B, Nagulan B. Efficacious separation of electron–hole pairs in CeO_2-Al_2O_3 nanoparticles embedded GO heterojunction for robust visible-light driven dye degradation. J Colloid Interface Sci. 2018;512:219-30. http://dx.doi.org/10.1016/j.jcis.2017.10.058.
58. Mokkelbost T, Kaus I, Grande T, Einarsrud MA. Combustion synthesis and characterization of nanocrystalline CeO2-based powders. Chem Mater. 2004;16(25):5489-94. http://dx.doi.org/10.1021/cm048583p.
59. Phoka S, Laokul P, Swatsitang E, Promarak V, Seraphin S, Maensiri S. Synthesis, structural and optical properties of CeO_2 nanoparticles synthesized by a simple polyvinyl pyrrolidone (PVP) solution route. Mater Chem Phys. 2009;115:423-8. http://dx.doi.org/10.1016/j.matchemphys.2008.12.031.
60. Nolan M, Parker SC, Watson GW. Vibrational properties of CO on ceria surfaces. Surf Sci. 2006;600(14):175-8. http://dx.doi.org/10.1016/j.susc.2006.05.015.